Oxidation pathway and kinetics of titania slag powders during cooling process in air

Wen-chao He[2,3], *Cheng-yi Ding*[4], *Xue-wei Lv*[1,2,3], *and Zhi-ming Yan*[5]

1) State Key Laboratory of Mechanical Transmissions, Chongqing University, Chongqing 400044, China

2) Chongqing Key Laboratory of Vanadium-Titanium Metallurgy and New Materials, Chongqing University, Chongqing 400044, China.

3) College of Materials Science and Engineering, Chongqing University, Chongqing 400044, China.

4) College of Metallurgical Engineering, Anhui University of Technology, Maanshan 243002, China.

5) WMG, University of Warwick, Coventry, CV4 7AL, UK.Corresponding author: Xue-wei Lv, Professor, Email: lvxuewei@cqu.edu.cn.

Abstract:

The oxidation pathway and kinetics of titania slag powders in air were analyzed through differential scanning calorimetry (DSC) and thermogravimetry (TG). The oxidation pathway of titania slag powders in air is divided into three stages according to three exothermic peaks and three corresponding mass gain stages displayed in the non-isothermal DSC and TG curves respectively. The isothermal oxidation kinetics of high titania slag powders with different sizes were analyzed through *ln-ln* analysis method. The entire isothermal oxidation process includes the following two stages. The kinetic mechanism of first stage is described as $f(\alpha) = 1.77(1 - \alpha)[-\ln(1 - \alpha)]^{(1.77-1)/1.77}$, $f(\alpha) = 1.97(1 - a)[-\ln(1 - a)]^{(1.97-1)/1.97}$, and $f(\alpha) = 1.18(1 - \alpha)[-\ln(1 - \alpha)]^{(1.18-1)/1.18}$; whereas the kinetic mechanism of second stage for all samples can be described as $[1 - (1 - \alpha)^{1/3}]^2 = kt$. The activation energies of titania slag powders with different sizes ($d_1 < 0.075$ mm, $0.125 < d_2 < 0.150$ mm, and $0.425 < d_3 < 0.600$ mm) at different reaction degrees are calculated. Under the current experimental conditions, the rate-controlling step at the first oxidation stage of all samples is a chemical reaction. The rate-controlling steps at the second oxidation stage are the chemical reaction and internal diffusion ($d_1 < 0.075$ mm) and the internal diffusion ($0.125 < d_2 < 0.150$ mm and $0.425 < d_3 < 0.600$ mm).

Keywords: high titania slag powder; oxidation pathway; isothermal oxidation kinetics; *ln-ln* analysis; activation energy; rate-controlling step

1. Introduction

The ilmenite resources deposited in Panzhihua, China are among the largest ilmenite reserves. The ilmenite reserves are approximately 0.87 billion tons (in TiO_2), accounting for about 35% of

the total resource worldwide [1]. The Panzhihua ilmenite concentrate can be processed into high titania slag by electric furnace smelting, which increases the TiO_2 content from 40−50wt% to more than 73wt%. The obtained high titania slag is the major material for TiO_2 pigment production with sulfate process. In 2018, the Chinese annual output of TiO_2 pigment reached approximately 2.95 million tons, of which more than 94% was manufactured via the sulfate process. High titania slag contains titanium suboxides (TiO, Ti_2O_3) and ferrous oxide (FeO), both of which can easily react with O_2 under air during the cooling process. In the sulfate process, the anosovite phase (M_3O_5) is easily dissolved in sulfuric acid, whereas the rutile phase (TiO_2) is insoluble in sulfuric acid. Therefore, the oxidation of titanium suboxide should be restricted during the cooling process to prevent the rutile phase formation.

The industrial manufacturing process of high titania slag powders includes smelting, trapping into a slag ladle, cooling in the ladle with a water spray, dropping from the slag ladle, crushing, and grinding. The molten high titania slag from the electric arc furnace was trapped into the slag ladle, and its surface was cooled with a water spray. After several hours, the cooled slag was dropped from the ladle, crushed, and ground to less than 0.075 mm. The acidolysis rate of high titania slag powders can reach up to 90% in the sulfate process. However, this industrial manufacturing process of high titania slag powders is low efficiency and consumes a large amount of energy and water. Thus, an effective method is needed to prepare high titania slag powders with high productivity, low water consumption, and low energy consumption.

Researchers have proposed a number of dry granulation processes to manufacture blast furnace slag particles, such as rotary disc atomizer, rotary drum atomizer, rotary cup atomizer (RCA), and rotary cylinder atomizer [2−6]. RCA technology, one of the most popular granulation

3

processes, was first introduced to treat slags [3], the heat of slag granules could be recovered to produce steam or hot water. Fig. 1 shows a novel high titania slag powder manufacturing process that utilizes RCA with air cooling.

Fig. 1. Novel high titania slag powder manufacturing process using RCA.

The rotational speed of RCA was first set at a target value, then the molten high titania slag was poured out from tundish and impinged onto RCA. The molten high titania slag was spread out to form droplets and then cooled and solidified into granules under air cooling. During the granulation process, part of the sensible heat was recovered from the off-gas.

To obtain high titania slag powders with high acidolysis rate, the oxidation behavior of industrial high titania slag in air should be first studied. Numerous studies have explored the physical and chemical properties of titania slag, whereas only a few researches have considered the oxidation kinetics of titania slag. The non-isothermal oxidation kinetics of three different kinds of high titania slags with high TiO_2 concentration was instigated by Deng et al. [7]. The total contents of the titanium oxide were 84.30 and 78.01wt%. In their study, the oxidation of high titania slag was divided into three stages, as follows: oxidation of titanium oxide with low reaction speed (T<673 K); oxidation of titanium oxide with moderate reaction speed (673 K<T<973 K);

4

and oxidation of titanium oxide and FeO with high reaction speed (T>973 K). The oxidation product of titanium oxide at the first stage caused a lattice distortion of the anosovite phase. The oxidation product of titanium oxide at the latter two stages were mainly the anatase phase (TiO_2) and the rutile phase (TiO_2), respectively. Li et al. investigated the isothermal oxidation kinetics of Ti-bearing slag with different Fe_2O_3 content in air using electromotive-force [8]. The variation of oxygen potential with time was obtained through an oxygen sensor of solid electrolyte. They believed that the controlling step of slag oxidation was the diffusion of oxygen in Ti-bearing slag. The activation energy of oxygen diffusion decreased from 159.7 kJ/mol to 111.5 kJ/mol when the Fe_2O_3 content varied from 0 to 8wt%, indicating that the kinetic conditions can be improved by adding an appropriate amount of iron oxide. Reaction Kinetics of isothermal and non-isothermal oxidation of titaniferous slag (total titanium oxide content was 51wt%) in air were examined by thermal gravimetric technique in Zhang et al. study [9]. In their study, an unreacted core shrinking model was used to describe titaniferous slag oxidation. The isothermal oxidation of high titania slag was divided into two stages. The controlling steps at the initial and latter stages were chemical-reaction-controlled and diffusion-controlled steps, respectively. The apparent activation energies were 19.62 and 30.05 kJ/mol, as calculated by the isothermal kinetics model formula. In addition, the controlling steps of non-isothermal oxidation process were chemical reaction at stage I (T<873 K), chemical reaction and diffusion at stage II (873 K<T<1023 K), and diffusion at stage III (T>1023 K). Przepiera et al. performed thermogravimetric (TG) analyses of the oxidation of QIT (QIT Fer et Titane Inc., Quebec, Canada) high titania slag (the total titanium content was 47.4wt%) in air [10]. The reaction proceeded in two stages. The activation energy was 55.42 kJ/mol at the first oxidation stage and 144.27 kJ/mol, which was approximately thrice greater than

5

that at the second stage.

Table 1.   Oxidation kinetics of titania slag powder by previous researchers

E/(kJ/mol)		Samples	Powder size (mm)	Experiment condition	T (K)	Reference
159.7−111.5		Ti-bearing slag TTi=13.79−14.99wt% TFe=0−5.6wt%	—	Isothermal	1713−1743	[8]
First stage	19.62	Panzhihua high titania slag TTi=30.57wt% TFe=10.19wt%	—	Isothermal	733−1318	[9]
Second stage	30.05					
First stage	55.42	QIT high titania slag TTi=47.40wt%, TFe=8.10wt%	$0.16<d_1<0.315$ $0.400<d_2<0.500$ $0.8<d_3<1.25$	Non-isothermal	293−1273	[10]
Second stage	144.27					

TTi: the total titanium, TFe: the total iron

However, the reaction mechanism was hardly considered in these researches. In addition, the activation energies reported in previous studies varied significantly, as shown in Table 1. The significant difference in results from various investigations may be due to differences in experimental conditions. The oxidation of titania slag is a gas-solid reaction chemically regarded as a gaseous oxidation reaction of titanium suboxides and ferrous oxide. The rate-controlling step of titania slag powders oxidation process can be obtained by an unreacted core model. The experimental conditions, including temperature, gas rate, as well as powder size, suppose to influence the reaction mechanism and activation energy by acting on the interphase reaction and gas internal diffusion. For example, in Zhang's study, the powder size of the high titania slag in the isothermal oxidation experiments was not mentioned [9]. In Przepiera et al.'s work, the activation energies were obtained by non-isothermal oxidation experiments [10]. Generally, the particle size of titania slag is required to less than 0.075 mm in the sulfate process to ensure a high acidolysis rate. A novel high titania slag powder manufacturing process that utilizes RCA with air

cooling is proposed in present work to meet the size requirement, as shown in Fig. 1. Thus, the oxidation behavior of industrial high titania slag less than 0.075 mm should be studied.

Therefore, the oxidation pathway and kinetics of the Panzhihua high titania slag powders with different sizes in air were investigated by DSC and TGA. Additionally, the activation energy as well as model function of the oxidation mechanism was obtained.

2. Experimental

2.1. Materials

Table 2 shows the chemical composition of high titania slag supplied by Panzhihua Steel Company. The high titania slag was ground into powders, screened to different sizes, and then used in the kinetic experiments. The X-ray diffraction (XRD) pattern reveals that anosovite ((Ti, Fe, Mg)$_3$O$_5$) was the main phase of the sample, as shown in Fig. 2.

Table 2. The chemical composition analysis results of high titania slag powder

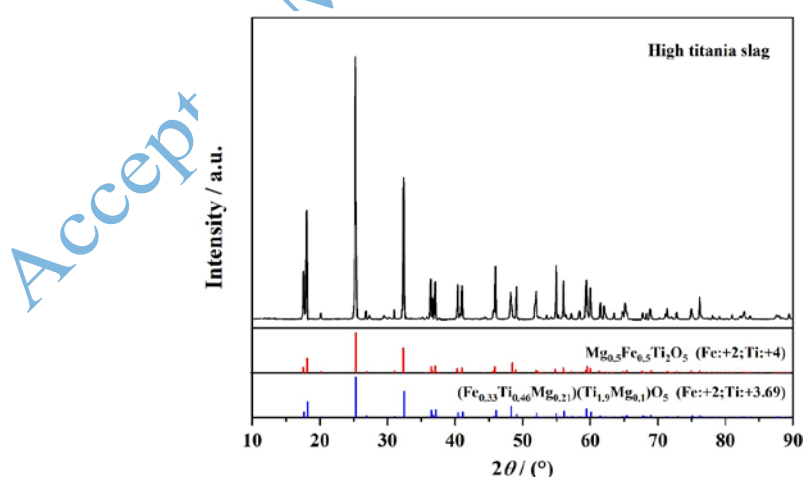| Composition	CaO	SiO$_2$	MgO	Al$_2$O$_3$	TiO$_2$	Ti$_2$O$_3$	TiO	FeO	MnO
Content (wt%)	1.76	5.58	8.33	2.25	55.60	13.73	4.00	7.83	0.92

Fig. 2. XRD pattern of industrial high titania slag powder.

2.2. TGA

DSC/TG measurements of the oxidation pathway and isothermal oxidation kinetics of the powdered high titania slag were carried out using the thermal analyzer (Netzsch STA 449C).

Oxidation pathway of high titania slag powder were investigated by non-isothermal TGA experiment. High titania slag powder (less than 0.075 mm) was heated from room temperature in air at 15 K·min^{-1}. The sample had an approximate mass of 10 mg and was loaded into a platinum crucible.

In the isothermal TGA experiments, high titania slag samples (10 mg) in a platinum crucible were heated to 1123 K, 1173 K, and 1223 K at 20 K·min^{-1}. High purity argon at 50 mL·min^{-1} was blown into reaction tube before the sample was heated. After the sample reached the target temperature, air at 50 mL·min^{-1} was flowed into the reaction tube. Table 3 shows the experimental scheme of isothermal oxidation. A blank test was also carried out to remove the influence of system error and buoyance force on the experiments. The DSC/TG results were obtained at isothermal oxidation stage.

Table 3.   Experimental scheme of isothermal oxidation

Raw material	Powder size (mm)	Oxidation temperature (K)
PZHTiS1	$d_1<0.075$ ($d_1<200$ mesh)	1123, 1173, 1223
PZHTiS2	$0.125<d_2<0.150$ ($120<d_2<100$ mesh)	1123, 1173, 1223
PZHTiS3	$0.425<d_3<0.600$ ($40<d_3<30$ mesh)	1123, 1173, 1223

PZHTiS: Panzhihua titania slag

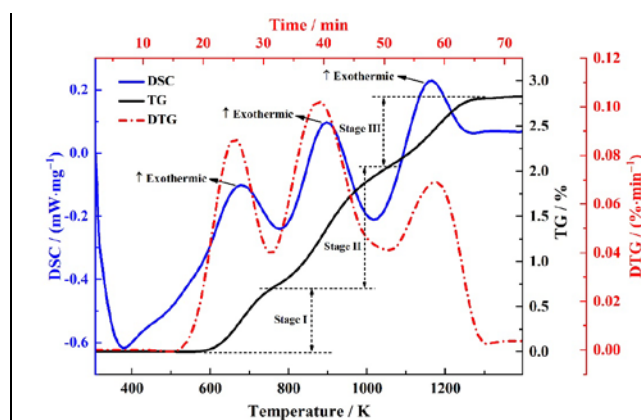# 3. Results and discussion

1.1. Oxidation pathway

Fig. 3.   DSC, TG, and DTG curves of high titania slag.
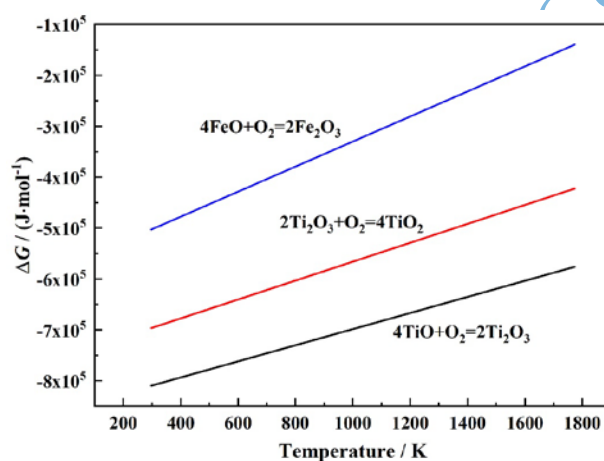

Fig. 4.   Gibbs-free energy of all oxidation reactions.
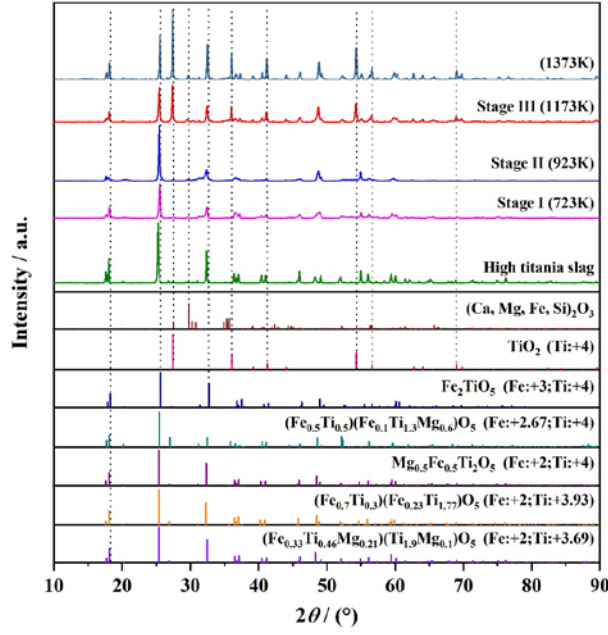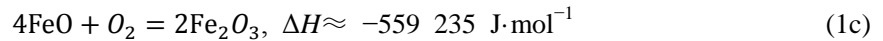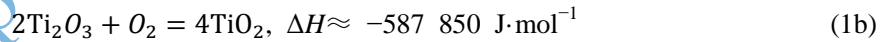
Fig. 5. XRD patterns of oxidized high titania slag at different temperatures.

Fig. 3 shows the DSC, TG, and differential TG (DTG) curves of high titania slag powder (less than 0.075 mm) reacting with air gas. The DSC curve of the sample displays three typical peaks, all of which are exothermic. The DTG curve also has three peaks. The three rate peaks for high titania slag oxidation corresponding to the three oxidation stages are presented in Fig. 3. The three oxidation stages can be expressed as follows:

$$4\text{TiO} + O_2 = 2\text{Ti}_2O_3, \ \Delta H \approx -857\ 462\ \text{J} \cdot \text{mol}^{-1} \tag{1a}$$

$$2\text{Ti}_2O_3 + O_2 = 4\text{TiO}_2, \ \Delta H \approx -587\ 850\ \text{J} \cdot \text{mol}^{-1} \tag{1b}$$

$$4\text{FeO} + O_2 = 2\text{Fe}_2O_3, \ \Delta H \approx -559\ 235\ \text{J} \cdot \text{mol}^{-1} \tag{1c}$$

The Gibbs-free energies of the oxidation reactions from 308 K to 1773 K were calculated using FactSage 6.2, as illustrated in Fig. 4. The Gibbs-free energy of all oxidation reactions are positive at the experimental temperatures, and TiO is easily oxidized in air, follow by Ti_2O_3 and FeO at the same temperature. Thus, the oxidation temperature is in the range of 500−755 K for

10

TiO to Ti_2O_3, 755−1055 K for Ti_2O_3 to TiO_2, and 1055−1400 K for FeO to Fe_2O_3. Fig. 5 shows the XRD patterns of oxidized titania slag at different temperatures.

The first rate peak is caused by the oxidation of titanium suboxide, and the corresponding TG curve interval (stage I) increases rapidly. Compared with that in the XRD pattern of industrial high titania slag, the relative content of the $(Fe_{0.33}Ti_{0.46})(Mg_{0.21}Ti_{1.9}Mg_{0.1}O_5)$ phase decreases in the XRD pattern of oxidized high titania slag at 723 K, and those of the $(Fe_{0.7}Ti_{0.3})(Fe_{0.23}Ti_{1.77})O_5$ and $Mg_{0.5}Fe_{0.5}Ti_2O_5$ phases increase. The phase transformation verifies the oxidation of titanium suboxide.

The second rate peak at approximately 893 K is caused by the oxidation of titanium suboxide. The increase in the TG curve interval at stage II is greater than that at stage I. Compared with the XRD pattern of the oxidized high titania slag at 723 K, the XRD pattern of oxidized high titania slag at 923 K shows that the relative contents of the $(Fe_{0.33}Ti_{0.46})(Mg_{0.21}Ti_{1.9}Mg_{0.1}O_5)$ and $(Fe_{0.7}Ti_{0.3})(Fe_{0.23}Ti_{1.77})O_5$ phases decrease, and the relative content of the $Mg_{0.5}Fe_{0.5}Ti_2O_5$ phase increases.

The third rate peak at approximately 1153 K is due to the oxidation of FeO and the formation of rutile phase. The relative content of the $Mg_{0.5}Fe_{0.5}Ti_2O_5$ phase in the XRD pattern of oxidized high titania slag at 1173 K is higher than in the XRD pattern of oxidized high titania slag at 923 K. In addition, the formation of the $(Fe_{0.5}Ti_{0.5})(Fe_{0.1}Ti_{1.3}Mg_{0.6})O_5$ and Fe_2TiO_5 phases verifies the oxidation of FeO. The rutile phase occurs at stage III, and its relative content increases rapidly.

The results of FactSage calculation, TGA and XRD reveal that the oxidation pathway of the high titania slag in air is TiO, Ti_2O_3 and FeO in order, and follow by the formation of the rutile phase.
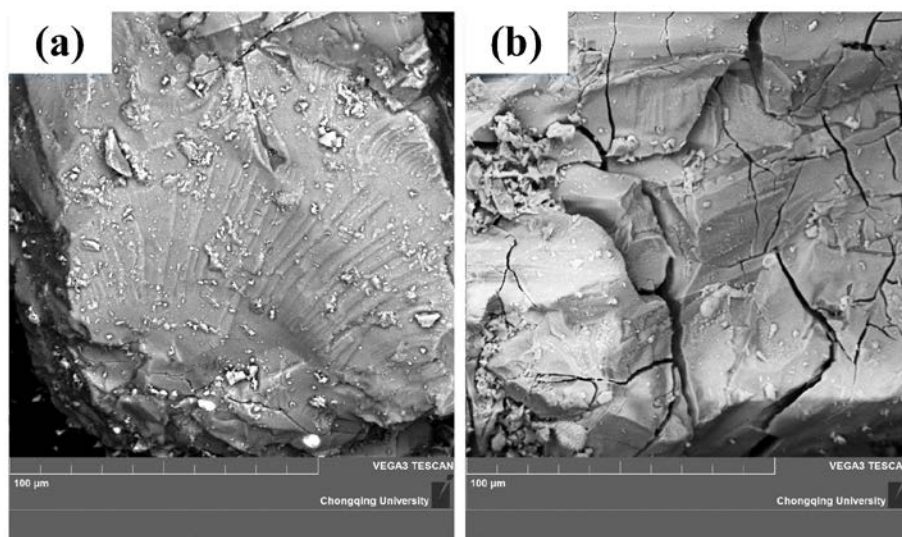
Fig. 6.   SEM morphology images of high titania slag (a) and oxidized high titania slag (b).

Fig. 6 provides the SEM morphology images of the original slag powder and oxidized slag powder. Fig. 6(a) depicts that the original slag powder has a smooth and compact surface, whereas the oxidized high titania slag powder displays lots of cracks on its surface, as shown in Fig. 6(b). Samal et al. believed that the cracks developed on the surface after heat treatment facilitated easy leaching in the sulfate process [11−12].

1.2. Isothermal TGA

3.2.1. TG analysis

TG curves of high titania slag samples reacting in air at different temperatures are illustrated in Fig. 7. The TG curves increase markedly when the air is blown into the sample tube and then increase gradually over time.
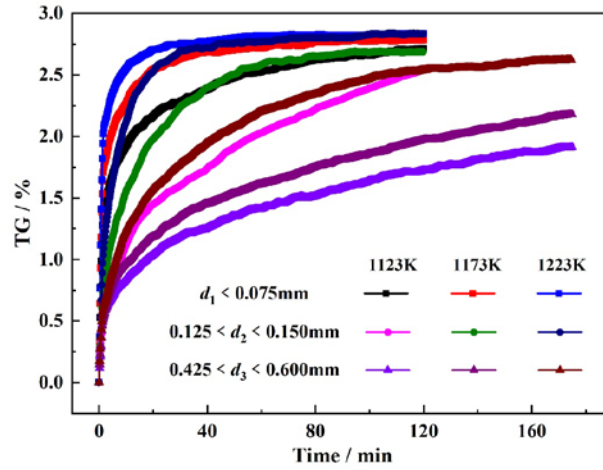
Fig. 7.   TG curves of high titania slag samples reacting in air.

The oxidation degree is described as the follow equation:

$$\alpha = \frac{\Delta m_t}{\Delta m_0} \tag{2}$$

here α represents the oxidation degree, Δm_t refers to the increase in the experimental TG percentages at a certain time, and Δm_0 refers to the theoretically increase in the TG percentages by the samples.

The relationship between oxidation degree and time at 1123−1223 K were calculated by Eq. (2). According to the chemical composition of titania slag, as shown in Table 2, the theoretically increase accounts for 3.40% when TiO, Ti_2O_3 and FeO are oxidized to TiO_2 and Fe_2O_3. Table 4 provides the maximum mass gain and oxidation degree of high titania slag samples.

Table 4.   Mass gain and oxidation degree of titania slag powders at different temperatures

Samples		$d_1 < 0.075$ mm	$0.125 < d_2 < 0.150$ mm	$0.425 < d_3 < 0.600$ mm
Mass gain (%)	1123 K	2.716	2.540	1.911
	1173 K	2.273	2.686	2.179
	1223 K	2.836	2.835	2.621
Oxidation degree (%)	1123 K	79.88	74.706	56.206
	1173 K	81.85	78.995	64.097
	1223 K	83.42	83.398	77.089

3.2.2. Reaction mechanism

On the basis of Avrami-Erofeev correlation, *ln-ln* analysis can be described as the relationship between oxidation degree (α), rate constant (k) and time (t) [13−16].`

$$1 - \alpha = e^{(-kt)^n} \tag{3}$$

here *n* refers to Avrami exponent.

By obtaining the natural logarithm on both sides of Eq. (3), Eq. (4) can be formulated as follows [17]:

$$\ln(-\ln(1-\alpha)) = n\ln t + n\ln k \tag{4}$$

$n\ln k$ and n are the intercept and slope of the fitting line.

As for solid-state reactions, the reaction models can be classified into geometric contraction, nucleation, reaction-order and diffusion models based on the mechanistic assumptions. A number of kinetic models have been proposed in previous work [18−19], as listed in Table 5.

Table 5.   Typical kinetic models

Functions	$f(\alpha)$	n
$A_3(\alpha)$	$[-\ln(1-\alpha)]^{1/3} = kt$	3.00
$A_2(\alpha)$	$[-\ln(1-\alpha)]^{1/2} = kt$	2.00
$R_3(\alpha)$	$-\ln(1-\alpha) = kt$	1.00
$R_2(\alpha)$	$1 - (1-\alpha)^{1/3} = kt$	1.07
$F_1(\alpha)$	$1 - (1-\alpha)^{1/2} = kt$	1.11
$D_1(\alpha)$	$\alpha^2 = kt$	0.62
$D_2(\alpha)$	$(1-\alpha)\ln(1-\alpha) + \alpha = kt$	0.57
$D_3(\alpha)$	$[1 - (1-\alpha)^{1/3}]^2 = kt$	0.54
$D_4(\alpha)$	$(1 - 2/3\alpha) - (1-\alpha)^{2/3} = kt$	0.57

The data fitting of all samples is described in Fig. 8. The entire oxidation process of the reaction at different temperature can be divided into two stages. According to Table 5, the slope values *n* of all samples at the first stage range from 1.10 to 2.00, the conversion function is

$f(\alpha) = n(1 - \alpha)[-\ln(1 - \alpha)]^{(n-1)/n}$, n=0.5, 1, 1.5, 2, 2.5, 3 and 4; the n values of all samples at the second stage are less than 0.54, and the conversion function is $[1 - (1 - \alpha)^{1/3}]^2 = kt$.
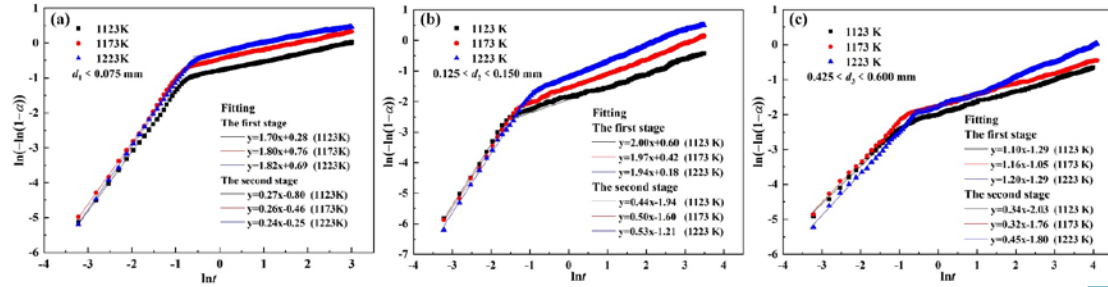

Fig. 8. **Avrami plots of $ln[-ln(1 - \alpha)]$ versus lnt: (a) d_1<0.075 mm, (b) 0.125<d_2<0.150 mm, and (c) 0.425<d_3<0.600 mm.**

Due to heterogeneous and complicated reaction of high titania slag, the experimental process of samples is disagree with the ideal process assumed in kinetic formula. Thus, conventional kinetic equations cannot be used to explain the kinetics mechanism of high titania slag oxidation. In all examples, the n values at the first stage are between 1.00 and 2.00, which deviated from the characteristic value n of the theoretical process. To settle the distortion between the real and ideal processes, an accommodation function $g(\alpha)$ was introduced by Koga and other researchers [20−22]. The actual kinetic formula is expressed by the following equation:

$$\square(\alpha) = f(\alpha)g(\alpha) \tag{5}$$

An alternative formula $h(\alpha)$ was introduced by researchers [22−24] to replace the general formula $f(\alpha)$. $H(\alpha)$ and $g(\alpha)$ are formulated as:

$$\square(\alpha) = N(1 - \alpha)[-\ln(1 - \alpha)]^{(N-1)/N} \quad 0.5 \leq N \leq 4 \tag{6}$$

$$g(\alpha) = \int_0^\alpha \left(d\alpha / \square(\alpha)\right) = [-\ln(1 - \alpha)]^{1/N} \quad 0.5 \leq N \leq 4 \tag{7}$$

In all samples, the characteristic values n at the first stage shown in Table 6 are equal to Avrami exponent N of actual kinetic equations [24]. Therefore, the average Avrami exponents' value of samples of a certain size is taken as N to represent actual reaction mechanism. Thus, the

actual reaction model of high titania slag powders of different sizes are described as:

$$\square(\alpha) = 1.77(1 - \alpha)[-\ln(1 - \alpha)]^{(1.77-1)/1.77} \tag{8}$$

$$\square(\alpha) = 1.97(1 - \alpha)[-\ln(1 - \alpha)]^{(1.97-1)/1.97} \tag{9}$$

and

$$\square(\alpha) = 1.18(1 - \alpha)[-\ln(1 - \alpha)]^{(1.18-1)/1.18} \tag{10}$$

Table 6 shows the kinetic models of all high titania slag powders.

Table 6.   Kinetic models of all high titania slag powders

Powder size (mm)	Period	Avrami exponent n	Functions
$d_1 < 0.075$	First stage	1.70−1.82	$f(\alpha) = 1.77(1 - \alpha)[-\ln(1 - \alpha)]^{(1.77-1)/1.77}$
	Second stage	0.24−0.27	$[1 - (1 - \alpha)^{1/3}]^2 = kt$
$0.125 < d_2 < 0.150$	First stage	1.94−2.00	$f(\alpha) = 1.97(1 - \alpha)[-\ln(1 - \alpha)]^{(1.97-1)/1.97}$
	Second stage	0.44−0.53	$[1 - (1 - \alpha)^{1/3}]^2 = kt$
$0.425 < d_3 < 0.600$	First stage	1.10−1.29	$f(\alpha) = 1.18(1 - \alpha)[-\ln(1 - \alpha)]^{(1.18-1)/1.18}$
	Second stage	0.32−0.45	$[1 - (1 - \alpha)^{1/3}]^2 = kt$

Fig. 9 illustrates the data fitting of selected kinetic equations for the two stages in the restricted range of $0.1 \leq \alpha \leq 0.75$ ($d_1 < 0.075$ mm). Table 7 shows the fitting parameters of all samples.
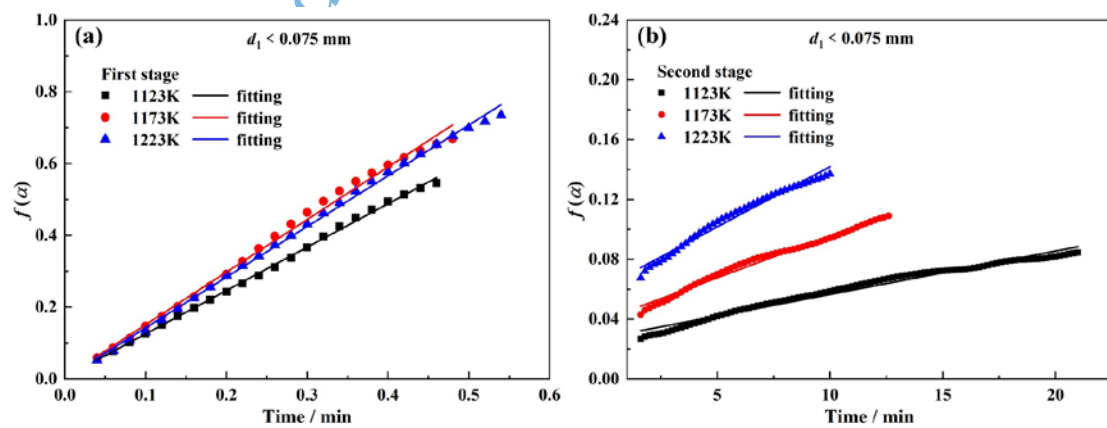

Fig. 9.   Data fitting of kinetic equations for the first stage (a) and second stage (b).

Table 7.   The values of the slope k and the corresponding Pearson's r

Powder size (mm)	Period		1123K	1173K	1223K
$d_1 < 0.075$	First stage	k	1.20	1.46	1.41
		r	0.999	0.997	0.999
	Second stage	k	0.0029	0.0056	0.0080
		r	0.989	0.993	0.990
$0.125 < d_2 < 0.150$	First stage	k	1.33	1.27	1.13
		r	0.999	0.999	0.998
	Second stage	k	0.0011	0.0028	0.0076
		r	0.999	0.997	0.999
$0.425 < d_3 < 0.600$	First stage	k	0.34	0.42	0.33
		r	0.997	0.999	0.999
	Second stage	k	0.00033	0.00051	0.0016
		r	0.994	0.990	0.996

3.2.3. Reaction activation energy

The kinetics basic equation [25] that describes the relationship between oxidation rate $(d\alpha/dt)$ and temperature (T):

$$\frac{d\alpha}{dt} = k(T)f(\alpha) \tag{11}$$

here $k(T)$ refers to rate constant, and $f(\alpha)$ refers to model function. The model function is effected by reaction mechanism, and the rate constant satisfied the Arrhenius equation:

$$k(T) = A\,exp(\frac{-E}{RT}) \tag{12}$$

where E refers to activation energy, A refers to pre-exponential factor, and R refers to gas constant. According to Eq. (12), Eq. (11) can be further described as:

$$\frac{d\alpha}{dt} = A\,exp(\frac{-E}{RT})f(\alpha) \tag{13}$$

We can formulate Eq. (14) by obtaining the natural logarithm on either side of Eq. (6):

$$\ln\frac{d\alpha}{dt} = \ln A - \frac{E}{RT} + \ln f(\alpha) \tag{14}$$

The relationship between $\ln(d\alpha/dt)$ and $1/T$ for high titania slag is determined through conversion method. According to Eq. (14), $-E/R$ can be obtained by the slope of the fitting line of

17

$\ln(d\alpha/dt)$ against $1/T$, as illustrated in Fig. 10 Then, the apparent activation energy is further calculated through slope value. Table 8 shows the activation energy of high titania slag powders at different conversion degrees. During isothermal oxidation of high titania slag, the oxidation reaction of titanium suboxides (TiO, Ti_2O_3), ferrous oxide (FeO) and the formation of rutile phase (TiO_2) take place simultaneously. Thus, the activation energy of slag samples calculated in present work is apparent activation energy.
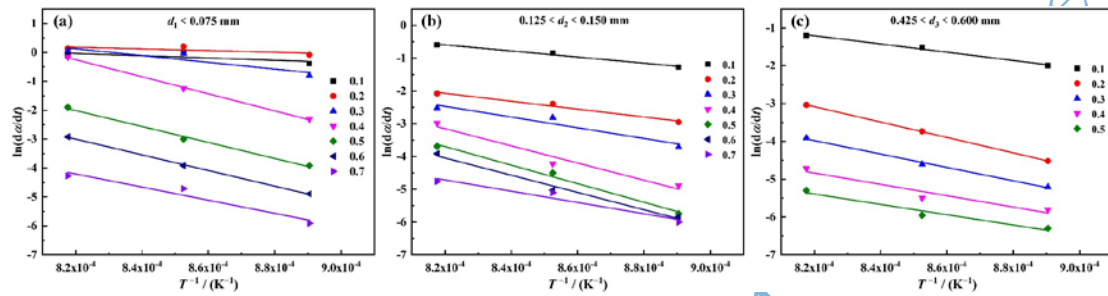

Fig. 10. Relationship of $\ln(d\alpha/dt)$ to 1/T by conversion method: (a) d_1<0.075 mm; (b) 0.125<d_2<0.150 mm; and (c) 0.425<d_3<0.600 mm.

Table 8. Reaction activation energy of all samples at different conversion degrees

	α	0.1	0.2	0.3	0.4	0.5	0.6	0.7
	d_1<0.075 mm	32.31	24.20	96.70	245.34	229.64	225.26	188.62
E/(kJ/mol)	0.125<d_2<0.150 mm	77.34	99.87	136.07	217.83	235.29	219.11	142.77
	0.425<d_3<0.600 mm	90.55	169.52	147.17	124.6	113.58	—	—

From Table 8, it can be observed that the reaction activation energy of all samples of different sizes initially increase and subsequently decrease as the conversion degree increases. The TiO and Ti_2O_3 are easily oxidized in air, thereby resulting in the low activation energy at the initial stage. Then, the activation energy is higher than that at the initial stage due to the limitation of the air diffusion. As the reaction proceeds, many cracks form on the surface of the oxidized layer of the samples, thereby promoting the oxidation process and decreasing the reaction activation energy.

3.2.4. Rate-controlling step

Given that air is gas, and the high titania slag powder is solid, the oxidation of high titania slag by air is a typical gas-solid reaction. Therefore, the rate-controlling step of high titania slag powders oxidation process can be obtained by an unreacted core model. The unreacted core model used in this study can be expressed by Eq. (15) [26]. Table 9 shows the relationship between restriction step and oxidation time [24].

$$\frac{r_0}{6} \cdot \frac{1}{D_e}\left[1 - 3(1-\alpha)^{2/3} + 2(1-\alpha)\right] + \frac{K}{1+K} \cdot \frac{1}{k}\left[1 - (1-\alpha)^{1/3}\right] = \frac{c_0 - c}{r_0 \rho}t \quad (15)$$

here r_0 refers to the powder's original radius, D_e refers to effective diffusion coefficient, k refers to reaction rate constant, K refers to equilibrium constant, ρ refers to the original oxygen concentration in slag powders, t refers to oxidation time, c and c_0 refer to gas concentration in equilibrium and on the surface of slag powder.

Table 9.   The relationship between restriction step and oxidation time

Oxidation time	$t = A[1 - (1-\alpha)^{1/3}]$	$t = B[1 - 3(1-\alpha)^{2/3} + 2(1-\alpha)]$	$t = A[1 - (1-\alpha)^{1/3}] + B[1 - 3(1-\alpha)^{2/3} + 2(1-\alpha)]$
Rate controlling step	Chemical reaction	Internal diffusion	Chemical reaction and internal diffusion

A and *B* are constant

The comparisons between internal diffusion–controlled step and chemical reaction–controlled step at the first stage of slag powders in restricted range of $0.1 \leq \alpha < 0.6$ ($d_1 < 0.075$ mm) are shown in Fig. 11. The first oxidation stage is controlled by chemical reaction considering that t is linear with $1 - (1-\alpha)^{1/3}$. According to the fitting results, the first oxidation stage of samples in the range of $\alpha \leq 0.1$ ($0.125 < d_2 < 0.150$ mm and $0.425 < d_3 < 0.600$ mm) is also controlled by a chemical reaction.
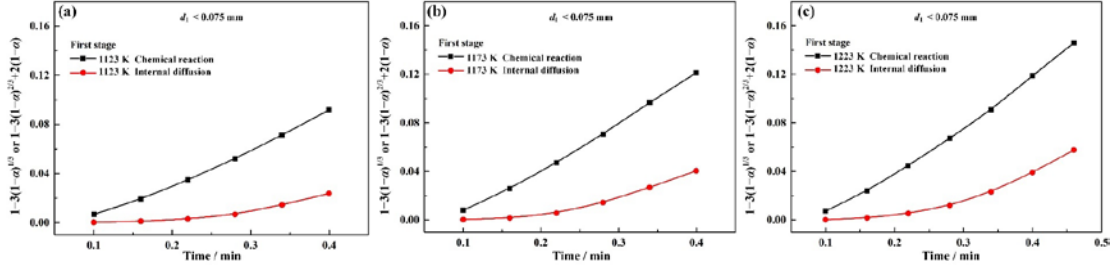
Fig. 11.   Comparisons between internal diffusion and chemical reaction at the first stage: (a) 1123 K; (b) 1173 K; and (c) 1223 K.

The comparisons between internal diffusion–controlled step and chemical reaction–controlled step at the second stage of slag powders are shown in Fig. 12. The samples of sizes in the range 0.125−0.150 mm in the restricted range of $0.2 \leq \alpha \leq 0.7$ and samples from 0.425 to 0.600 mm in the restricted range of $0.2 \leq \alpha \leq 0.5$ display that t is linear with $[1 - 3(1 - \alpha)^{2/3} + 2(1 - \alpha)]$. The controlling step of the rate of the second oxidation stage for these samples was internal diffusion. Samples less than 0.075 mm in the restricted range of $\alpha < 0.75$, $1 - (1 - \alpha)^{1/3}$ and $[1 - 3(1 - \alpha)^{2/3} + 2(1 - \alpha)]$ are linearly correlated with t.

By simplifying Eq. (15), Eq. (16) can be burned as the following equation:

$$\frac{t}{1-(1-\alpha)^{1/3}} = t_D \left[1 + (1 - \alpha)^{1/3} - 2(1 - \alpha)^{2/3}\right] + t_C \qquad (16)$$

here t_C and t_D refer to complete oxidation times when the oxidation is controlled by chemical reaction and internal diffusion, respectively.

$$t_D = \frac{\rho r_0^2}{6 D_e (c_0 - c)} \qquad (17)$$

$$t_C = \frac{\rho r_0 K}{k(1+K)(c_0 - c)} \qquad (18)$$

Fig. 13 shows a mixed controlled model at different temperatures. Thus, the oxidation of samples with less than 0.075 mm is controlled by both internal diffusion and chemical reaction.
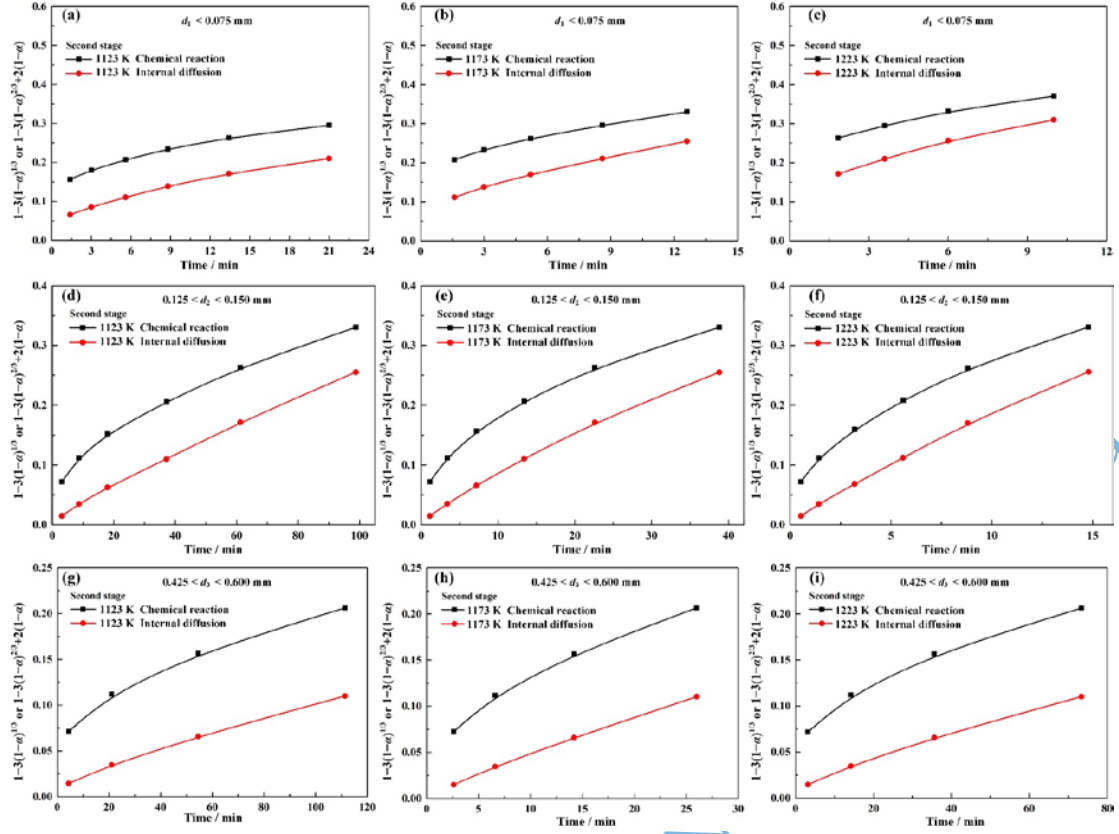
20

Fig. 12.   Comparisons between internal diffusion and chemical reaction at second stage: (a) d_1<0.075 mm, 1123 K; (b) d_1<0.075 mm, 1173 K; (c) d_1<0.075 mm, 1223 K; (d) 0.125<d_2<0.150 mm, 1123 K; (e) 0.125<d_2<0.150 mm, 1173 K; (f) 0.125<d_2<0.150 mm, 1223 K; (g) 0.425<d_3<0.600 mm, 1123 K; (h) 0.425<d_3<0.600 mm, 1173 K; and (i) 0.425<d_3<0.600 mm, 1223 K.
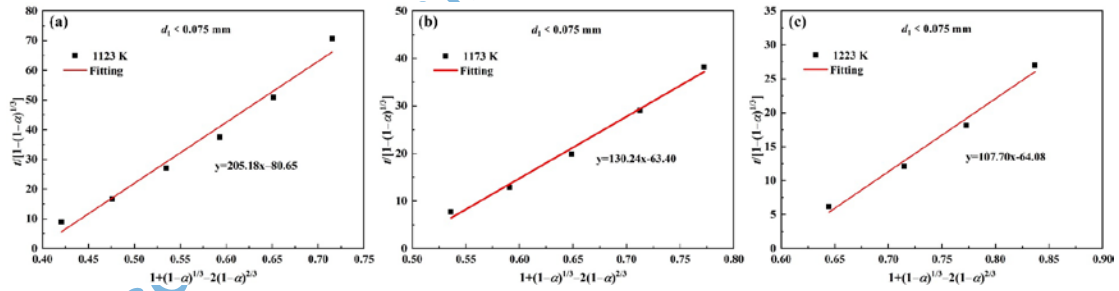

Fig. 13.   Mixed-control model under (a) 1123 K; (b) 1173 K; and (c) 1223 K.

Based on Fig. 11, the first oxidation stage of all titania slag samples (d_1<0.075 mm, 0.125<d_2<0.150 mm, and 0.425<d_3<0.600 mm) is controlled by a chemical reaction. As for a gas-solid reaction, temperature mainly contributes to the interphase reaction in the oxidation

process [27]; powder size also contributes to the interphase reaction due to different specific surface area [7]. According to Fig. 12 and Fig. 13, the rate-controlling step at the second oxidation stage include internal diffusion and chemical reaction (d_1<0.075 mm) and internal diffusion (0.125<d_2<0.150 mm and 0.425<d_3<0.600 mm). As for slag samples less than 0.075 mm, the distance from reaction interface to the surface of slag powder is relatively short, thereby the effect of air internal diffusion on oxidation behavior in the second stage is restricted due to its small powder size.

4. Conclusions

(1) The results of FactSage calculation, TGA and XRD indicate that the oxidation pathway of the high titania slag in air is TiO, Ti_2O_3 and FeO in order, follow by the formation of the rutile phase.

(2) The entire process of the isothermal oxidation is divided into two stages. At the first stage, the oxidation kinetic mechanism of all samples (d_1<0.075 mm, 0.125<d_2<0.150 mm, and 0.425<d_3<0.600 mm) can be described as $f(\alpha) = 1.77(1-\alpha)[-\ln(1-\alpha)]^{(1.77-1)/1.77}$, $f(\alpha) = 1.97(1-a)[-\ln(1-a)]^{(1.97-1)/1.97}$, and $f(\alpha) = 1.18(1-\alpha)[-\ln(1-\alpha)]^{(1.18-1)/1.18}$, respectively. At the second stage, the conversion function for all samples (d_1<0.075 mm, 0.125<d_2<0.150 mm, and 0.425<d_3<0.600 mm) is $[1-(1-\alpha)^{1/3}]^2 = kt$.

(3) The activation energies of titania slag powders with different sizes (d_1<0.075 mm, 0.125<d_2<0.150 mm, and 0.425<d_3<0.600 mm) at different reaction degrees are calculated.

22

(4) Under the current experimental conditions with temperature ranging from 1123 K to 1223 K, the rate-controlling step at the first oxidation stage of all samples is a chemical reaction. The rate-controlling step at the second oxidation stage include internal diffusion and chemical reaction ($d_1<0.075$ mm) and internal diffusion ($0.125<d_2<0.150$ mm and $0.425<d_3<0.600$ mm).

Acknowledgment

Reference

[1] Y.J. Zhang, T. Qi, and Y. Zhang, A novel preparation of titanium dioxide from titanium slag, *Hydrometallurgy*, 96(2009), p. 52.

[2] K.M. Lee and P.J. Park, Estimation of the environmental credit for the recycling of granulated blast furnace slag based on LCA, *Resour. Conserv. Recycl.*, 44(2005), p. 139.

[3] S.J. Pickering, N. Hay, T.F. Roylance, and G.H. Thomas, New process for dry granulation and heat recovery from molten blast-furnace slag, *Ironmaking Steelmaking*, 12(1985), p. 14.

[4] T. Mizuochi, T. Akiyama, T. Shimada, E. Kasai, and J.I. Yagi, Feasibility of rotary cup atomizer for slag granulation, *ISIJ Int.*, 41(2001), No. 12, p. 1423.

[5] Y. Kashiwaya, I.N. Yutaro, and T. Akiyama, Development of a rotary cylinder atomizing method of slag for the production of amorphous slag particles, *ISIJ Int.*, 50(2010), No. 9, p. 1245.

[6] Y. Kashiwaya, I.N. Yutaro, and T. Akiyama, Mechanism of the formation of slag particles by the rotary cylinder atomization, *ISIJ Int.*, 50(2010), No. 9, p. 1252.

[7] G.Z. Deng and X. Chen, The oxidation of high titania slag, *Iron Steel Vanadium Titanium*, 2(1985), p. 41.

[8] L.S. Li, G.Q. Li, T.P. Lou, Y.C. Che, and Z.T. Sui, Study on oxidation kinetics of Ti-enriched slag by electromotive force, *Acta Metal. Sin.*, 36(2000), No. 6, p. 642.

[9] L. Zhang, G.Q. Li, and Z.T. Sui, Oxidation kinetics of titaniferous slag, *Chin. J. Nonferrous Met.*, 12(2002), No. 5, p. 1069.

[10]   A. Przepiera and M. Jabłoński, Thermal transformations of high titania slag of high titania content, *J. Therm. Anal. Calorim*, 74(2003), p. 631.

[11]   S. Samal, B.K. Mohapatra, P.S. Mukherjee, and S.K. Chatterjee, Integrated XRD, EPMA and XRF study of ilmenite and titania slag used in pigment production, *J. Alloys Compd.*, 474(2009), p. 484.

[12]   S. Samal, B.K. Mohapatra, and P.S. Mukherjee, The effect of heat treatment on titania slag, *J. Miner. Mater. Char. Eng.*, 9(2010), No. 9, p. 795.

[13]   A. Khawam and D.R. Flanagan, Solid-state kinetic models: basics and mathematical fundamentals, *J. Phys. Chem. B*, 110(2006), p. 17315.

[14]   H.H. Sheu, L.C. Hsiung, and J.R. Sheu, Synthesis of multiphase intermetallic compounds by mechanical alloying in Ni-Al-Ti system, *J. Alloys Compd.*, 469(2009), p. 483.

[15]   Y.P. Shen, H.H. Hng and J.T. Oh, Formation kinetics of Ni–15% Fe–5% Mo during ball milling, *Mater. Lett.*, 58(2004), p. 2824.

[16]   C.X. Li, X.W. Lv, J. Chen, X.Y. Liu, and C.G. Bai, Kinetics of titanium nitride synthesized with Ti and N_2, *Int. J. Refract. Met. Hard Mater*, 52(2015), p. 165.

[17]   S.S. Tan, A.H. Su, W.H. Li, and E.L. Zhou, New insight into melting and crystallization behavior in semicrystalline poly(ethylene terephthalate), *J. Polym. Sci., Part B: Polym. Phys.*, 38(2015), p. 53.

[18]   Q. Lin, N. Chen, Y. Wen, and R.M. Liu, Kinetics of hydrogen absorption in hydrogen storage alloy, *Int. J. Miner. Metall. Mater.*, 4(1997), No. 2, p. 34.

[19]   J.D. Hancock and J.H. Sharp, Method of comparing solid-state kinetic data and its application to the decomposition of kaolinite, brucite, and $BaCO_3$, *J. Am. Ceram. Soc.*, 55(1972), p.74.

[20]   N. Koga, Kinetic analysis of thermoanalytical data by extrapolating to infinite temperature, *Thermochim. Acta*, 258(1995), p. 145.

[21]   J. Šesták, Diagnostic limits of phenomenological kinetic models introducing the accommodation function, *J. Therm. Anal.*, 36(1990), p. 1997.

[22]   R. Ozao and M. Ochiai, Fractal Reaction in solids : reaction functions reconsidered, *J. Ceram. Soc. Jpn.*, 101(1993), p. 263.

[23]   N. Koga, J. Malek, J. Sestak, and H. Tanaka, Data treatment in non-isothermal kinetics and diagnostic limits of phenomenological models, *Netsu Sokutei*, 20(1993), p. 210.

[24]   X.D. Gao, J.S. Wang, W. Lv, J.Y. Xiang, and X.W. Lv, The isothermal reduction kinetics of chromium-bearing vanadium–titanium magnetite sinter, *Can. Metall. Q.* 58(2019), p. 177.

[25]   R.C. Mccune and P. Wynblatt, Calcium segregation to a magnesium oxide (100) surface, *J. Am. Ceram. Soc.*, 66(1983), p. 111.

[26]   J. Tang, M.S. Chu, F. Li, Y.T. Tang, Z.G. Liu, and X.X. Xue, Reduction mechanism of high-chromium vanadium-titanium magnetite pellets by H_2-CO-CO_2 gas mixtures, *Int. J. Miner. Metall. Mater.*, 22(2015), No. 6, p. 562.

[27]   C.Y. Ding, X.W. Lv, S.W. Xuan, K. Tang, and C.G. Bai, Isothermal reduction kinetics of powdered hematite and calcium ferrite with CO-N_2 gas mixtures, *ISIJ Int.*, 56(2016), No. 12, p. 2118.

二级学科名称：（080602） 钢铁冶金。